Journal of Applied Polymer Science

Fundamental Influences on Quasistatic and Cyclic Material Behavior of Short Glass Fiber Reinforced Polyamide Illustrated on Microscopic Scale

Julia Brunbauer,[1] Andreas Mösenbacher,[2] Christoph Guster,[2] Gerald Pinter[1]

[1]Department of Polymer Engineering and Science, Institute of Materials Science and Testing of Polymers, University of Leoben, Otto-Gloeckel-Straße 2, 8700 Leoben, Austria

[2]Department Product Engineering, University of Leoben, Franz-Josef-Straße 18, 8700 Leoben, Austria

Correspondence to: J. Brunbauer (E-mail: julia.brunbauer@unileoben.ac.at)

ABSTRACT: In this work, the influences of fiber orientation and weld lines on the morphological structures and the mechanical behavior of polyamide 6.6 (PA6.6-GF35) are investigated. In quasistatic and fatigue tests tensile and 3-point-bending loads are applied. Test temperatures vary between RT and 150°C. Two different specimen types are produced by using injection moulding process to create different fiber orientations as well as weld lines. Fiber orientations are determined using computer tomography. Scanning electron microscopy is used to investigate fracture surfaces of tested specimens. Results show that mechanical properties and morphological structures depend highly on fiber orientation and temperature. Transversely oriented fibers in weld lines result in brittle failure mechanisms and decreased mechanical properties. Different stress distributions in the specimens under tensile and flexural loads have influence on the material behavior as well. © 2014 Wiley Periodicals, Inc. J. Appl. Polym. Sci. **2014**, *131*, 40842.

KEYWORDS: fibers; mechanical properties; morphology; polyamides; properties and characterization

Received 20 January 2014; accepted 6 April 2014
DOI: 10.1002/app.40842

INTRODUCTION

Short fiber reinforced plastics (SFRP) have found an increasing number of applications due to their high mechanical strength and the possibility of easy and fast production of complex geometries by injection moulding process. To meet lightweight requirements, SFRP are sometimes used to replace automotive components traditionally made of metal materials such as engine air intake manifold, steering column bracket, and cooling fan housing.[1] As a result of the production process, SFRP parts possess usually two specific characteristics: first, the fibers added for reinforcement are oriented depending on part geometry and production process. Second, many parts made of SFRP contain weld lines.

The strengthening effect of fibers in a thermoplastic matrix is strongly influenced by fiber length and the relation between fiber orientation and the direction of stresses acting on the component. Fiber orientation results from a complex interaction of two effects during the injection moulding process: on one hand, shear flow, which tends to align fibers in proximity of the mould walls usually observed in case of converging streamlines. Conversely, extensional flow, which arranges the fibers perpendicular to the polymer flow in case of diverging streamlines and at the flow front.[2,3] Mechanical properties of SFRP are moreover affected by process parameters such as melt temperature, mould temperature, injection pressure, injection speed, and hold pressure.[4]

Many experimental attempts have been made to characterize the complex fiber orientation in injection moulded fiber reinforced composites. Reflected light microscopy, X-ray radiography or tomography, and electron microscopy are only some of the methods used for detection of fiber orientation. In 1987, Advani and Tucker reported about the use of tensors for two-dimensional (2D) description and prediction of fiber orientation and developed the Advani-Tucker tensor.[5] Other 2D image analysis techniques for detection of fiber orientations have been reported.[6–8] X-ray microtomography can be a powerful tool for 3D analysis of glass fiber reinforced composites and nonwoven textiles.[9] Even in simple injection moulded parts such as thin plates, fiber orientation is not uniform but shows a layered structure, consisting of at least a core and two shell layers.[3,10] Figure 1 illustrates fiber orientation in an injection moulded plate compared to an injection moulded standardized testing specimen.

Weld lines emerge in injection moulded parts if the fronts of two or more flows of molten material meet. This is the case if the material flow needs to surround mould cores or if different injection gates are used to fill the cavity. Varying wall thicknesses causing partially faster and slower melt fronts can result

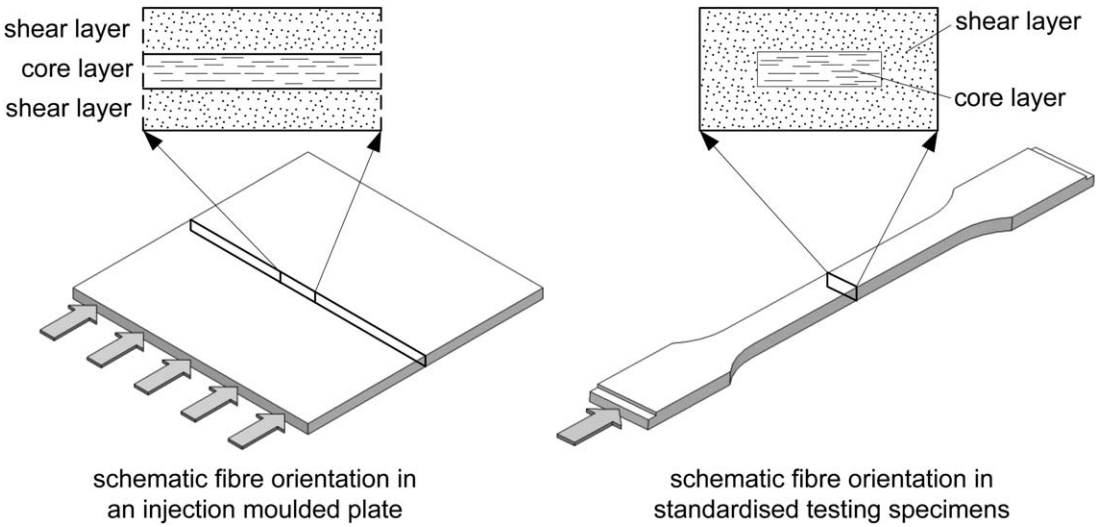

Figure 1. Schematic fiber orientation in an injection moulded plate (left) and in a standardized testing specimen (right) with shear (longitudinal fiber orientation) and core layer (transversal fiber orientation) (referring to [11]).

in weld lines as well.[12] Added fibers are often arranged perpendicular to the flow direction at the flow fronts. As a result, weld lines are usually mechanical weak points in structural parts. Mechanical properties of weld lines are somewhere in the range of the unreinforced matrix material or even below.[1,13] However, little knowledge exists about actual fiber orientation tensors in weld lines which would be of particular interest for adequate part and lifetime estimations.

Fiber orientation and weld lines are only two characteristics affecting the mechanical properties of SFRP that need to be taken into account under fatigue loads, which are very likely to occur in automotive applications. Additionally, environmental conditions such as humidity, operating medium, and aging agents can affect the mechanical properties of SFRP as well and were investigated in detailed studies.[14–16] Moreover temperature, stress state, stress concentrations, and fiber orientations affect quasistatic as well as fatigue behavior of SFRP.[17–22]

Fatigue life estimation of real parts has to take into account loading types and stress concentrations. Fatigue analysis by local stress concept published by Eichlseder presents a simulation model for stress-life (S-N) curves which enables the fatigue life estimation with results of finite element calculations by taking into account irregular stress distributions in real parts.[23] This model has been successfully applied for life time estimation of injection moulded components made of SFRP.[19,22,24]

This article is part of a work aimed to integrate fiber orientation and weld lines in a fatigue life estimation model based on the stress gradient concept by Eichlseder.[23] Experimental data, on which life time estimations are based, are presented in this article. Two specimen types made of short fiber reinforced polyamide 6.6, containing 35 wt % glass fibers were tested under quasistatic and fatigue loads at different temperatures. Tensile and 3-point-bending loads were applied to create different stress gradients in the specimens. Fiber orientations were characterized with computer tomography (CT) and orientation tensors were determined. Additionally, fracture surfaces of specimens failed in mechanical tests were investigated with scanning electron microscopy (SEM). Results showed the influence of the two different kinds of specimen production on the mechanical properties and their decrease with raising test temperature. Failure mechanisms and mechanical properties could be correlated with shear and core layer distribution resulting from the injection moulding process.

EXPERIMENTAL

The investigated material is a short fiber reinforced polyamide 6.6, containing 35 wt % glass fibers (designation PA6.6-GF35). Fibers have a nominal diameter of 10–15 μm and an average fiber length in the range of 50–500 μm (measured by CT). The glass transition temperature of the material estimated by dynamic-mechanical analysis is around 65°C.

To investigate the influence of different fiber orientations caused by the specimen production process (Figure 1) on the mechanical properties and morphological material structures, specimens were produced in two different ways. The first specimen type should possess shear and core layers along the full width of the specimen. Therefore, plates of 100 × 100 mm size with 4 mm thickness were injection-moulded through a T-shaped injection gate. Specimens referring to DIN EN ISO 527-2 were milled out from these plates under two angles $\theta = 0°$ and $\theta = 90°$.[25] Three specimens were milled from plates in fiber direction ($\theta = 0°$) and named with left, middle, right and two specimens transverse to fiber direction ($\theta = 90°$), named with above and below (Figure 2). Because of their dimensions according to DIN EN ISO 527-2 but shortened specimen length limited by the plate size, these specimens were entitled "short standardized testing specimens."[25]

The second specimen type was injection moulded to create a core layer surrounded by shear layers (Figure 1). Therefore, "standardized testing specimens" according to testing standard DIN EN ISO 527-2 with testing cross-section of 10 × 4 mm were injection moulded.[25] Additionally, this specimen geometry

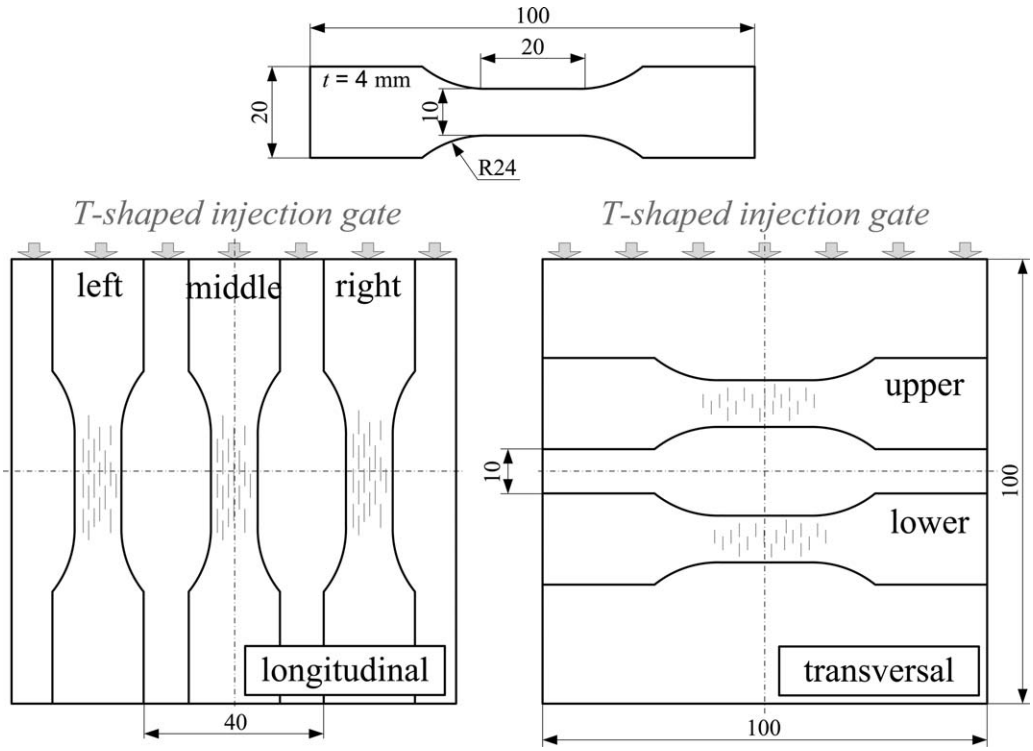

Figure 2. Specimen type 1: sampling and dimensions of short standardized testing specimens milled from injection moulded plates in mm.

could be produced with weld lines in the middle of the specimen to characterize the influence of weld lines. By varying the injection film gates from either injecting mould only from one side or mould injection from both sides, the second specimen type was produced with and without weld lines (Figure 3).

Specimens were delivered from producer in "dry as moulded" conditions. Each specimen was weighed and stored in indoor climate after delivery. Weighing of specimens was repeated in certain intervals and immediately before testing. Therefore, moisture content in each specimen was known when conducting the respective mechanical tests. By testing specimens not in "dry as moulded" conditions, the test results may reproduce a more application oriented behavior. Figure 4 illustrates mass change in the specimens caused by water absorption versus storing time before testing in hours.

Quasistatic tensile tests with short standardized specimens at 23 and 90°C and with standardized testing specimens at 90°C were carried out on an allround-line materials (tensile/compression) test machine Zwick/Roell Z010®. The test machine was equipped with a load cell of 10 kN and contacting high accuracy strain measuring device by Zwick/Roell in loading direction. Standardized testing specimens at RT and at 150°C as well as short standardized specimens at 150°C were tested on a servohydraulic test machine Instron 8501® with a maximum test force of ±10 kN. The test machine was equipped with a load cell of 10 kN and extensometers for strain measurement by Instron. For standardized testing specimens, the initial clamping length was 110 mm, for short standardized testing specimens milled from plates it was 40 mm. The tensile modulus, E_t, was determined according to the DIN EN ISO 527-1 standard.[26] The three test temperatures were chosen well below (23°C) and above (90 and 150°C) the glass transition temperature. For the tests at 90 and 150°C a temperature chamber with a digital temperature controller was used.

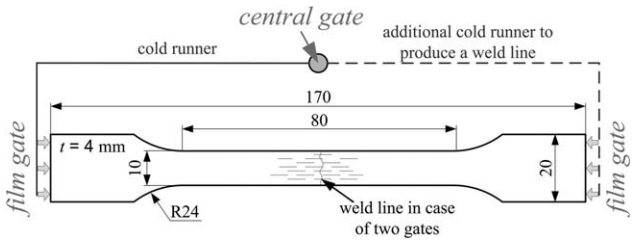

Figure 3. Specimen type 2: sampling and dimensions of injection moulded standardized testing specimens in mm, produced with and without weld lines.

Quasistatic 3-point-bending tests with standardized testing specimens at 23°C were carried out on the aforementioned test machine Zwick/Roell Z010® according to DIN EN ISO 178 standard.[27] Radius of loading edge and radius of supports was 5 mm. The distance between the supports was 64 mm which equalled 16 times the nominal thickness of 4 mm. The test machine was equipped with a load cell of 10 kN and a contacting high accuracy strain measuring device by Zwick/Roell recording the flexural strength and the strain at failure. Quasistatic tensile as well as 3-point-bending tests were conducted with a defined crosshead strain rate $d\varepsilon/dt = 0.909\%\ \text{min}^{-1}$ which is approximately equivalent a testing speed of $v = 1\ \text{mm min}^{-1}$ for an initial clamping length of 110 mm.

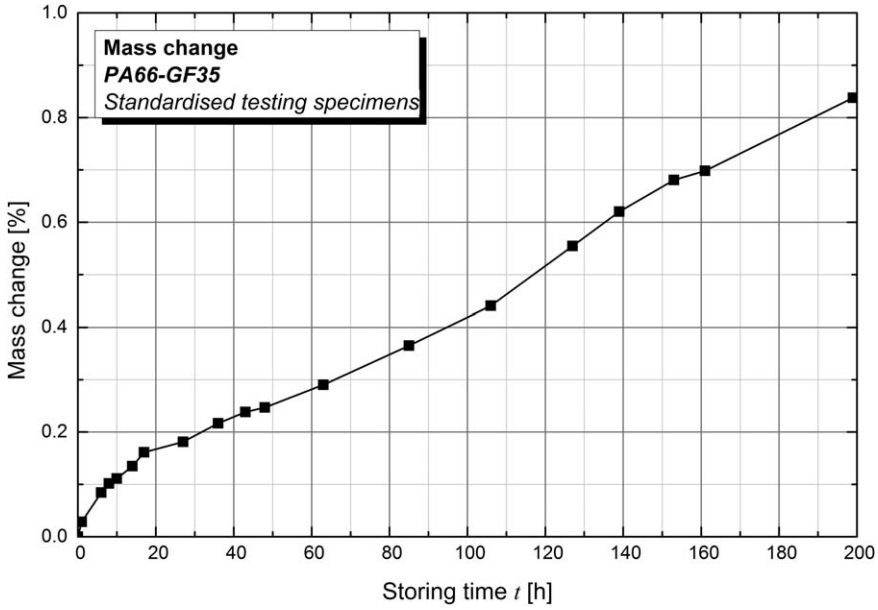

Figure 4. Mass change versus storage time in hours to estimate moisture at time of testing.

Tensile/tensile fatigue tests with short standardized testing specimens at 23°C were carried out on a MTS858® servo-hydraulic test machine, equipped with a load cell of 15 kN, tensile/tensile fatigue tests at 150°C were conducted on a electromechanical test machine, equipped with a load cell of 15 kN. The fatigue tests were executed under load control, applying a sinusoidal load function with constant amplitude. Tensile/tensile fatigue tests were performed keeping a constant load ratio $R = P_{min}/P_{max} = 0.1$. In preliminary tests, the influence of frequency on hysteric heating and fatigue behavior was evaluated. Based on preliminary tests and to shorten testing time, a temperature increase of less than 5°C referred to the test temperature was accepted. Depending on the applied load, test frequencies were varied between 4 and 10 Hz. During all tensile/tensile fatigue tests at 23°C the temperature at the specimen surface was monitored by an infrared sensor.

Flexural fatigue tests under 3-point-bending load were carried out on a MTS858® servo-hydraulic test machine, equipped with a load cell of 1 kN. Radii and distance between the supports was identical to the quasistatic 3-point-bending tests. The fatigue tests were executed under load control, applying a sinusoidal load function with constant amplitude. All bending fatigue specimens were tested at 23°C. Flexural tests were performed with a constant load ratio $R = 0.1$. Again, load frequency was chosen in such way

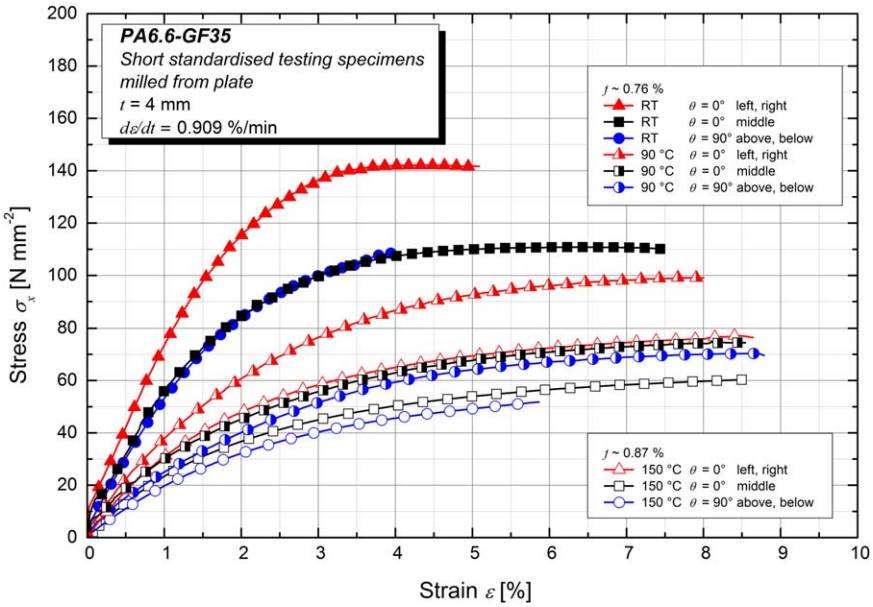

Figure 5. Comparison of stress-strain curves for short standardized testing specimens milled from plates under $\theta = 0°$ and $\theta = 90°$ at RT, 90 and 150°C under quasistatic tensile load. [Color figure can be viewed in the online issue, which is available at wileyonlinelibrary.com.]

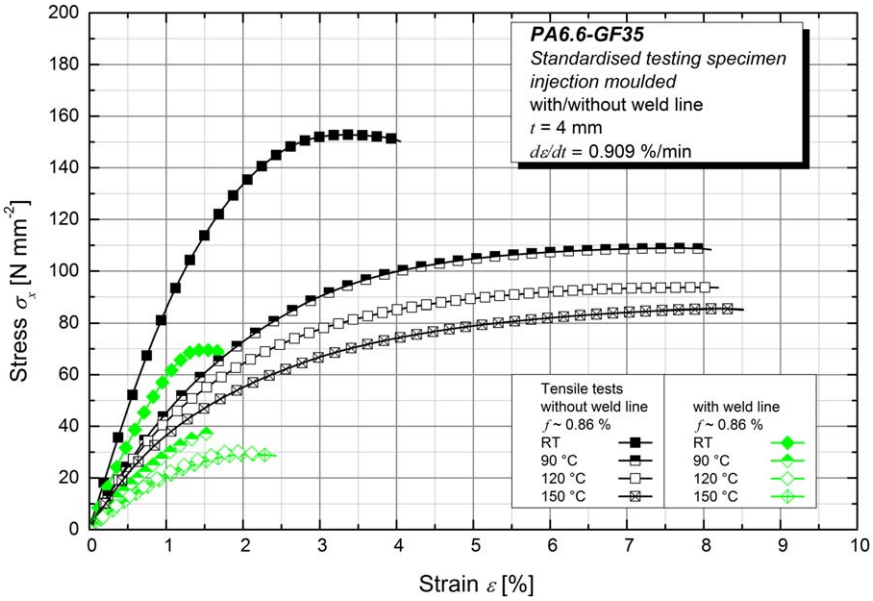

Figure 6. Comparison of stress–strain curves for injection moulded standardized testing specimens at RT, 90, 120, and 150°C with and without weld lines under quasistatic tensile load. [Color figure can be viewed in the online issue, which is available at wileyonlinelibrary.com.]

that the temperature increase due to hysteretic heating was not more than 5°C referred to the test temperature. Due to the smaller highly stressed material volume compared to the tensile/tensile fatigue tests and less hysteretic heating all flexural fatigue tests could be performed with 10 Hz. Tensile/tensile fatigue tests at RT as well as 3-point-bending fatigue tests were executed in a test laboratory with standard atmosphere (23°C, 50% relative humidity). It is believed that at typical room humidity moisture absorption is negligible during test times.[21] Thus, no control of the relative humidity was operated during the tests.

RESULTS AND DISCUSSION

Quasistatic Tests

The influence of fiber orientation in quasistatic tensile tests performed with short standardized testing specimens milled from plates will be discussed first. Representative stress-strain curves measured at RT, 90 and 150°C are presented in Figure 5. Short standardized testing specimens milled from the left and right sides of the plates had higher tensile strengths than specimens milled from plates' middles. Similiarities between tensile strengths of specimens milled from the middle of the plates in

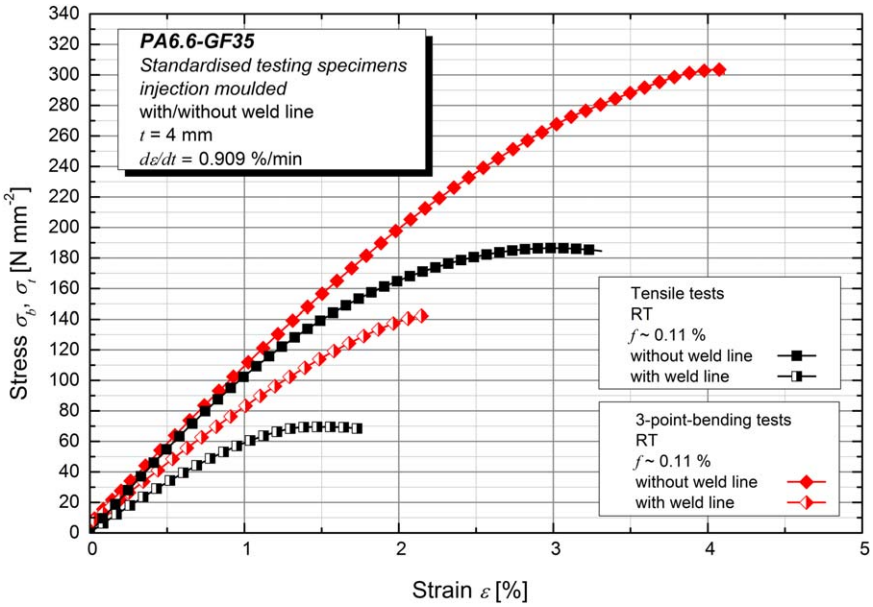

Figure 7. Comparison of stress–strain curves for injection moulded standardized testing specimens at RT with and without weld lines under tensile and flexural load. [Color figure can be viewed in the online issue, which is available at wileyonlinelibrary.com.]

Table I. Temperature T, Orientation θ, Moisture f, and Average Values of Tensile Strengths σ_M and Tensile Modulus E_t for Quasistatic Tests Under Tensile Load ($d\varepsilon/dt = 0.909\%/\text{min}$)

Specimen	T (°C)	θ (°)	f (%)	σ_M (N mm^{-2})	E_t (N mm^{-2})
Short standardised testing specimen	23	0	0.76	144	6360
Short standardised testing specimen	90	0	0.76	100	3982
Short standardised testing specimen	150	0	0.87	77	3706
Short standardised testing specimen	23	90	0.76	107	5625
Short standardised testing specimen	90	90	0.76	69	2818
Short standardised testing specimen	150	90	0.87	50	2188
Standardised testing specimen	23	0	0.11	186	11152
Standardised testing specimen	23	0	0.86	152	9975
Standardised testing specimen	90	0	0.76	109	5296
Standardised testing specimen	120	0	0.87	94	5199
Standardised testing specimen	150	0	0.86	86	4592
Standardised testing specimen with weld line	23	0	0.11	66	6672
Standardised testing specimen with weld line	23	0	0.86	63	6161
Standardised testing specimen with weld line	90	0	0.76	37	3273
Standardised testing specimen with weld line	120	0	0.87	31	2630
Standardised testing specimen with weld line	150	0	0.86	29	2490

fiber direction ($\theta = 0°$) and specimens transverse to fiber direction ($\theta = 90°$) result from the distinctive core layer in the plates illustrated in Figure 1. Breaking strains of specimens in fiber direction ($\theta = 0°$) were lower compared to specimens with $\theta = 90°$. Specimens tested at RT in fiber direction ($\theta = 0°$) behaved in a quite ductile way in contrast to published studies which can be related to the moisture content $f = 0.76\%$ in the specimens.[20] The stress-strain curves at 90 and 150°C confirm that the tensile strengths of specimens taken from the middle of the plates are lower compared to the edge areas as monitored at RT. Injection moulded standardized testing specimens without weld lines failed in a ductile manner in quasistatic tests as presented in Figure 6. Specimens with weld lines on the contrary failed in a brittle way even at high temperatures.

All specimens showed decreasing tensile strengths and increasing strains with increasing temperature, which is consistent with literature. Though, the effect of raising temperature in tensile tests was stronger for standardized testing specimens without weld lines and short standardized testing specimens milled from plates compared to standardized specimens with weld lines. In specimens with weld lines, the temperature increase from 120 to 150°C caused only little further decrease in tensile strength.

The comparison between injection moulded standardized testing specimens with and without weld lines under tensile and 3-point-bending loads is presented in Figure 7. σ_b and σ_t are the stress limits of bending and the stress limit of tension, respectively. Stress limits under flexural load for specimens with and without weld lines are higher than respective stress limits under tensile loading which can be ascribed to the stress gradients in the bending specimens and the resulting plastification and support effects. Additionally, the stress gradient in specimens under bending loads results in less loading in the core zone.

In addition to the quasistatic stress-strain curves, Tables I and II list type of specimens, fiber orientation, testing temperature, moisture content, and mechanical properties in greater detail. Standardized testing specimens with and without weld lines were tested with two different moisture contents in tensile tests. The results are listed in Table I to illustrate strong influence of moisture on mechanical properties. Table II compares flexural moduli for standardized testing specimens with and without weld lines. Flexural moduli were decreased as a result of weld lines.

Fatigue Tests

All fatigue data were analyzed by the classical stress-life approach referring to ASTM E 739-91.[28] In the diagrams shown later, data are drawn in terms of nominal stress amplitude $\sigma_{a,n}$ versus the number of cycles to failure N. Test results are reported in double logarithmic diagrams. Specimens that passed 5×10^6 cycles without failure were usually stopped. These

Table II. Temperature T, Orientation θ, Moisture f, and Average Values of Flexural Strengths at Break σ and Flexural Modulus E_f for Quasistatic Tests under Flexural Loads

Specimen	T (°C)	θ (°)	f (%)	σ (N mm^{-2})	E_f (N mm^{-2})
Standardised testing specimen	23	0	0.11	305	10600
Standardised testing specimen with weld line	23	0	0.11	145	7980

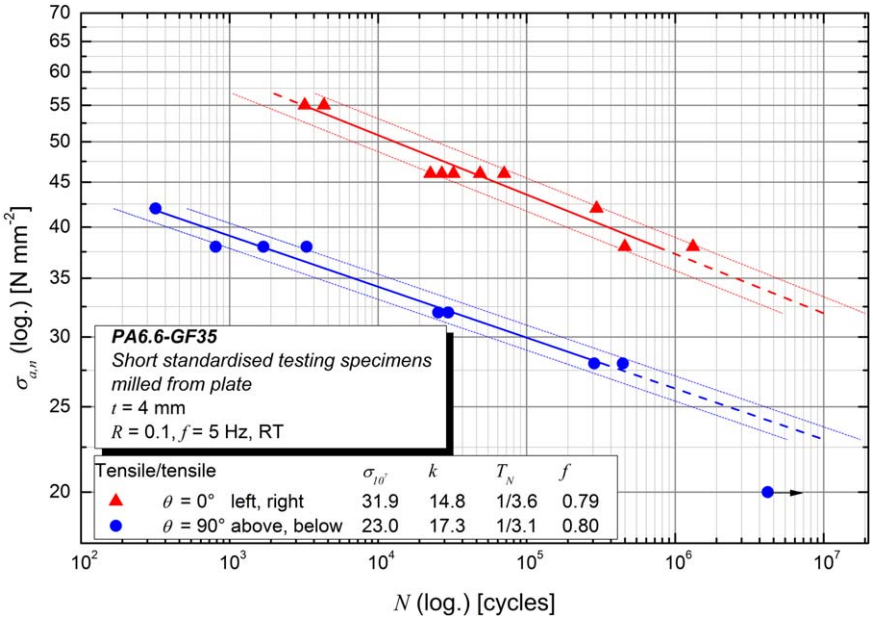

Figure 8. Uniaxial fatigue curves at RT for specimens milled from plates ($\theta = 0°$ and $\theta = 90°$) for loading ratio $R = 0.1$. [Color figure can be viewed in the online issue, which is available at wileyonlinelibrary.com.]

runouts are marked in the diagrams with an arrow. The S-N curves can be described by the endurable fatigue strength at 10^7 cycles, $\sigma_{a,10^7}$ and the inclination k. N_i describes the endurable number of cycles at the stress level $\sigma_{a,i}$.[23]

$$N_i = 10^7 \times \left(\frac{\sigma_{a,10^7}}{\sigma_{a,i}} \right)^k \quad (1)$$

The values for σ_a at $N = 10^7$ ($\sigma_{a,10^7}$), the inclination of the fatigue line (k), the scatter width of fatigue test results (T_N), and the moisture content (f) are listed in the respective diagrams. For fatigue tests with short standardized testing specimens in fiber direction only specimens from the left and right sides of the plates are illustrated.

Figure 8 presents the influence of fiber orientation ($\theta = 0°$ and $\theta = 90°$) at RT for loading ratio $R = 0.1$. The results for fatigue tests with loading ratio $R = -1$ are illustrated in Figure 9. Short standardized testing specimens milled from plates in fiber direction bore higher stress amplitudes than specimens milled transverse to fiber direction for both loading ratios. Stress amplitudes under alternating loads were higher compared to

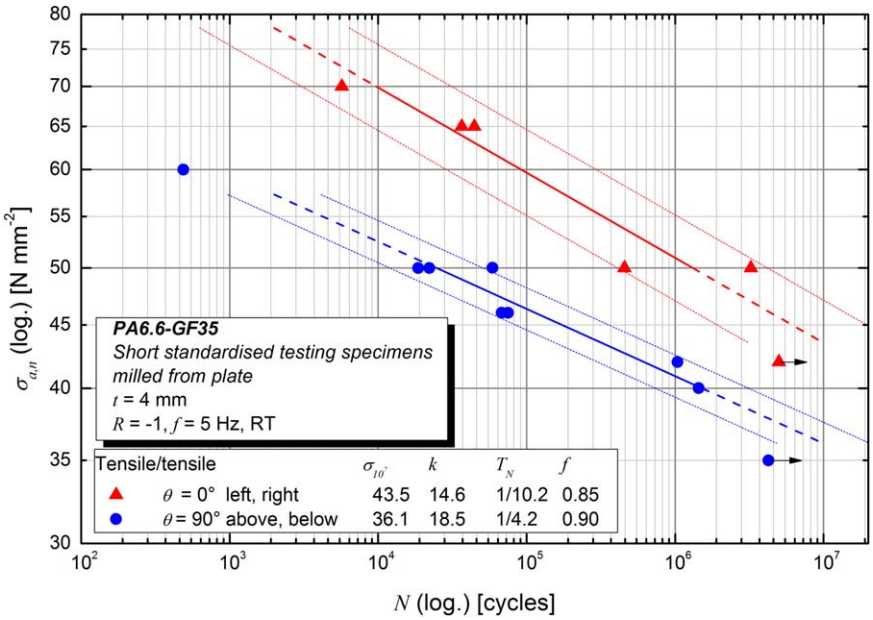

Figure 9. Uniaxial fatigue curves at RT for specimens milled from plates angles ($\theta = 0°$ and $\theta = 90°$) for loading ratio $R = -1$. [Color figure can be viewed in the online issue, which is available at wileyonlinelibrary.com.]

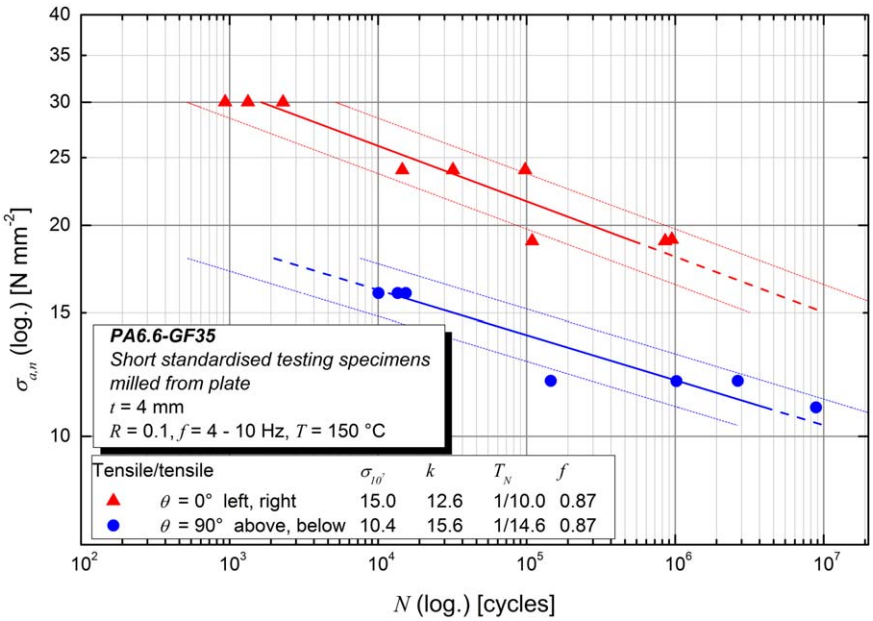

Figure 10. Uniaxial fatigue curves at 150°C for specimens milled from plates ($\theta = 0°$ and $\theta = 90°$) for loading ratios $R = 0.1$. [Color figure can be viewed in the online issue, which is available at wileyonlinelibrary.com.]

pulsating tensile loads. Figure 10 presents the influence of temperature on cyclic strength for loading ratio $R = 0.1$ investigated with short standardized testing specimens milled from plates. At 150°C fatigue strengths of short standardized specimens in and transverse to fiber direction decreased because of increasing ductility in the PA 6.6 matrix material when testing beyond the glass transition temperature. The inclinations of the performed fatigue tests did not show either dependence of temperature or of orientation.

Figure 11 compares fatigue results of standardized specimens with and without weld lines under tensile to results under bending loads. σ_{bf} and σ_{tf} are the fatigue limit of bending and the fatigue limit of tension loads, respectively. Due to the bigger shear layer in injection moulded standardized testing specimens (Figure 1) and consequently, more fibers which are aligned in load direction under tensile loads, standardized testing specimens possessed higher mechanical properties compared to short standardized specimens (Figure 8). Nominal stress amplitude at

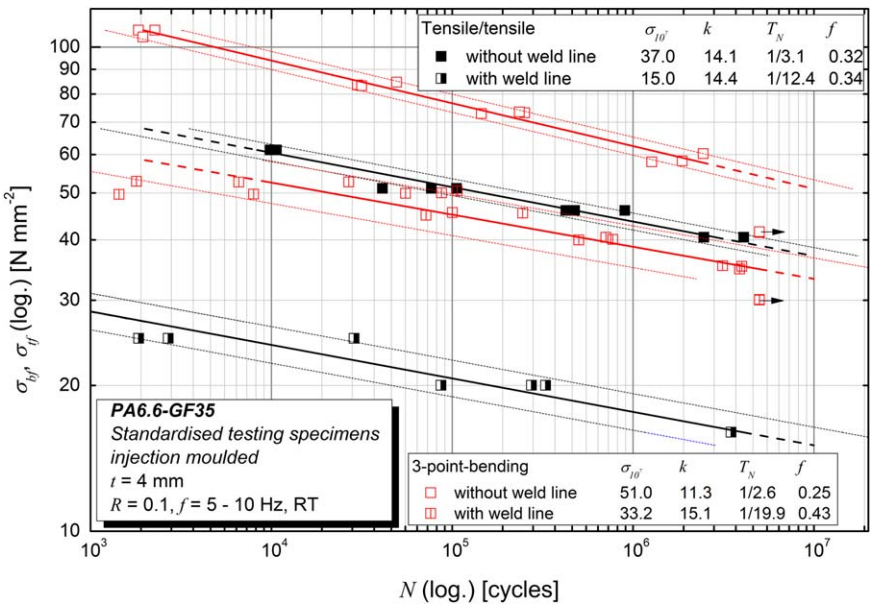

Figure 11. Uniaxial fatigue curves at RT for injection moulded standardized specimens with and without weld line for loading ratio $R = 0.1$ under tensile and flexural load. [Color figure can be viewed in the online issue, which is available at wileyonlinelibrary.com.]

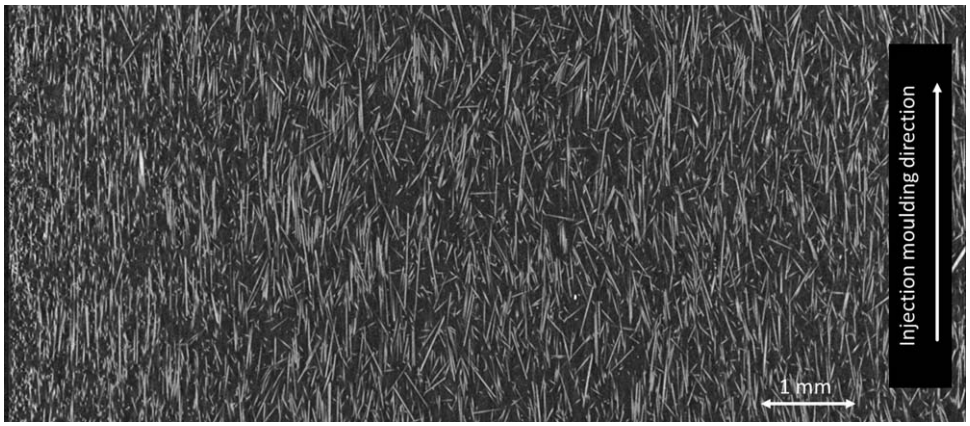

Figure 12. CT-photograph of a nontested standardized testing specimen without weld line (front view).

$N = 10^7$ raised from 31.9 N mm^{-2} for short standardized testing specimens to 37 N mm^{-2} for standardized testing specimens. Influence of specimen geometries on the inclinations of the S-N curves was not found. Fatigue strengths of standardized testing specimens under flexural load were higher than under tensile loads because of the stress gradient and less highly stressed volume under flexural loads as explained in relation with monotonic tests. Nominal stress amplitudes at $N = 10^7$ under flexural loads were almost 40% higher for specimens without weld lines and more than 120% for specimens with weld lines compared to tensile loads. This emphasized the influence of transversely oriented fibers in weld lines under tension loads. Under flexural as well as tension loads specimens always failed in the weld lines.

Fiber Orientations and Weld Lines with Computer Tomography. Fiber orientations in nontested specimens were investigated with CT. CT pictures provided not only information about the qualitative orientation of fibers but also the actual orientation vector of each fiber. The intact specimens were scanned from front to the back side. Because of scanning through the specimens the illustrated figures provide front views of the fiber orientation in the middle of the specimens. Injection moulding direction is marked in the figures. Figure 12 illustrates fiber orientation in a standardized specimen without weld line. Fibers are well aligned in injection moulding direction and, therefore, in load direction in uniaxial tests. In contrast, the formation of fibers in a weld line is illustrated in Figure 13. The injection moulded melt fronts meet at the weld line. In the weld line itself, fibers are oriented transverse to injection moulding direction. The CT photographs emphasize the decreasing influence of weld lines on mechanical properties.

Fracture Surfaces with Scanning Electron Microscopy. In addition to CT, fracture surfaces of specimens failed under quasistatic and cyclic loads were investigated with SEM to create better understanding for the influence of fiber orientations and weld lines at different temperatures on the damage mechanisms. A few examples of fracture surfaces of specimens failed under fatigue loads are presented. In the following pictures marked with a) and b) are SEM photographs taken at the shear layer of the failure surface according to Figure 1, whereas c) and d) show the core layer of the fatigue fracture surfaces. The illustrated short standardized testing specimens in fiber direction were milled from the left and right sides of the plates.

In Figure 14 the core layer fracture surface of a short standardized testing specimen milled from plate in fiber direction ($\theta = 0°$, RT, $R = 0.1$, $N = 296289$) is presented. Fibers in this

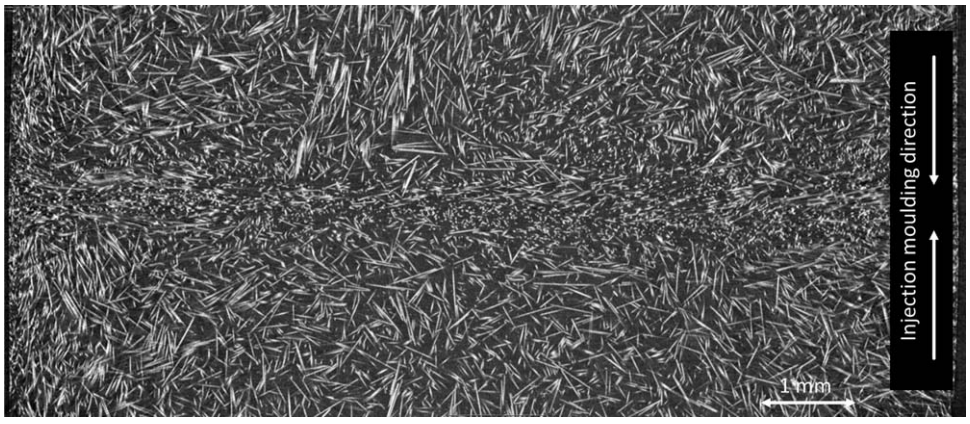

Figure 13. CT-photograph of a nontested standardized testing specimen with weld line (front view).

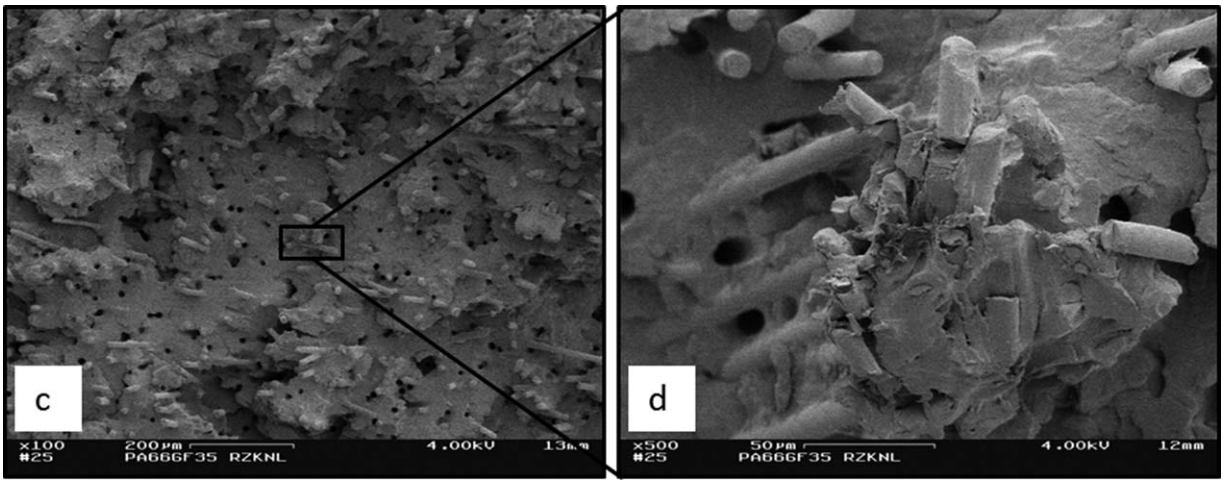

Figure 14. Fracture surface of PA6.6-GF35 short standardized fatigue specimen, orientation angle $\theta = 0°$, RT, $\sigma_a = 42$ N mm^{-2}, $R = 0.1$, $N = 296289$, (core layer): c) core layer with 100× magnification and d) core layer with 500× magnification.

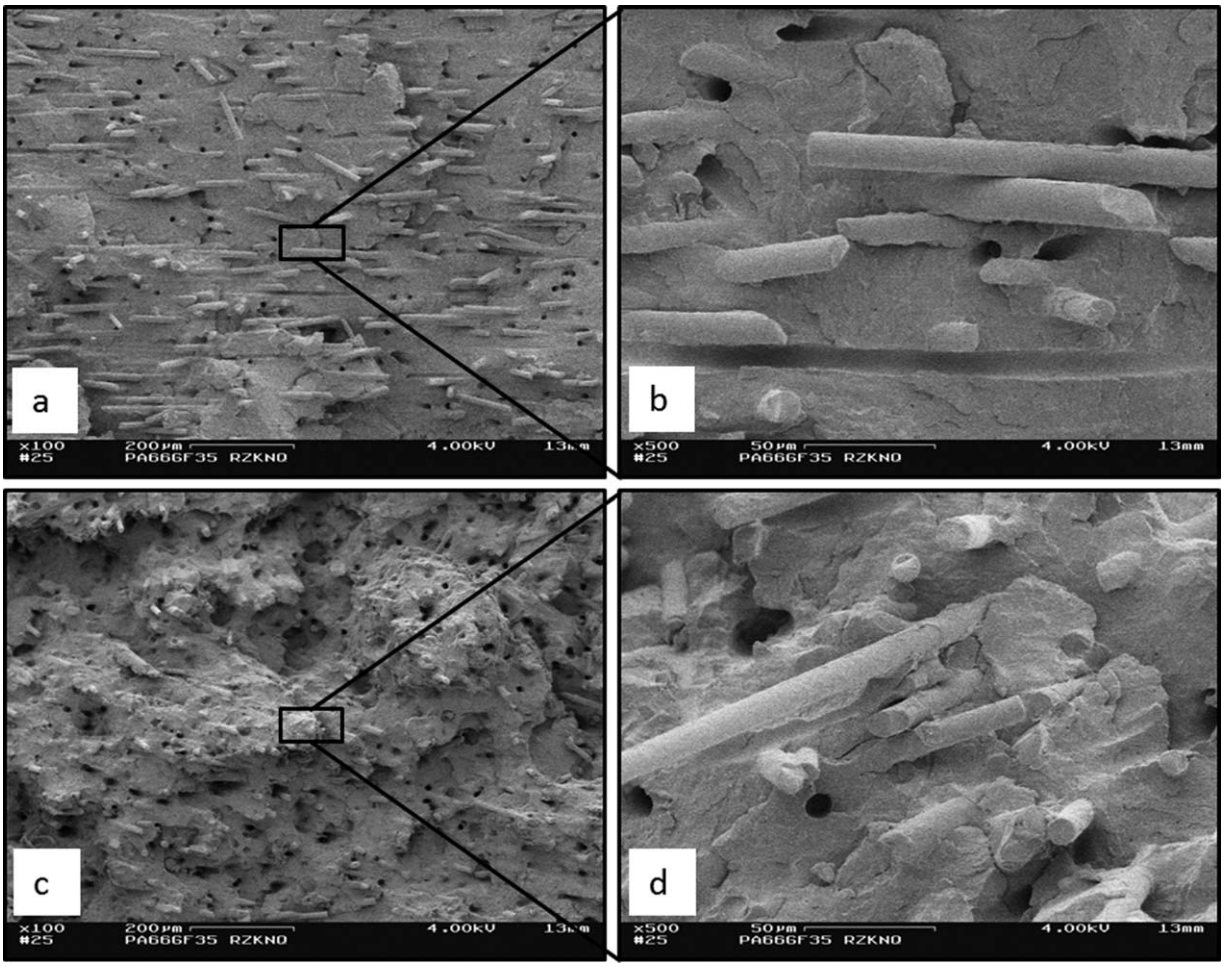

Figure 15. Fracture surface of PA6.6-GF35 short standardized fatigue specimen, orientation angle $\theta = 90°$, RT, $\sigma_a = 28$ N mm^{-2}, $R = 0.1$, $N = 285298$ (shear and core layer): a) shear layer with 100× magnification, b) shear layer with 500× magnification, c) core layer with 100× magnification, and d) core layer with 500× magnification.

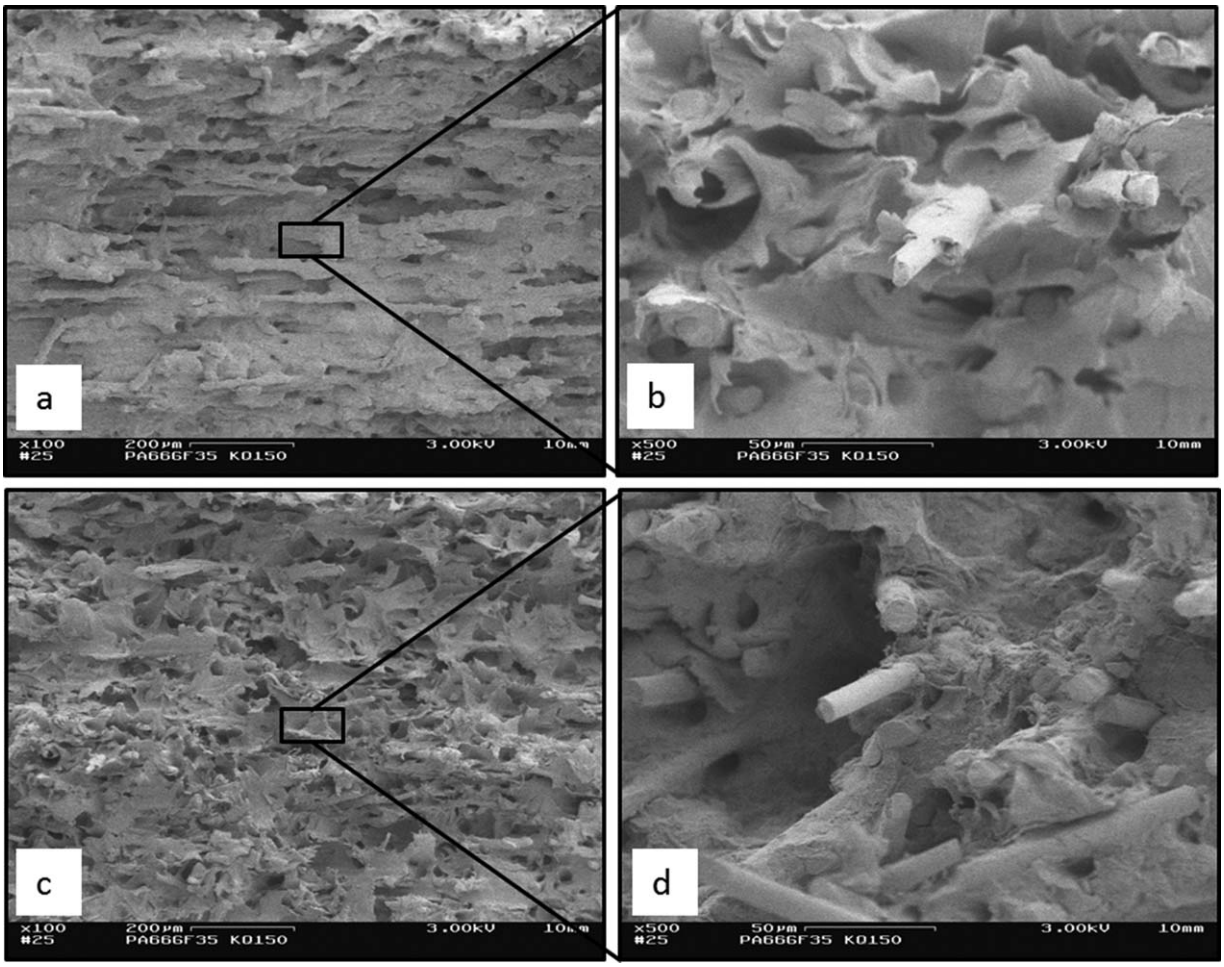

Figure 16. Fracture surface of PA6.6-GF35 short standardized fatigue specimen, orientation angle $\theta = 90°$, $T = 150°C$, $\sigma_a = 12$ N mm^{-2}, $R = 0.1$, $N = 1020000$ (shear and core layer): a) shear layer with 100× magnification, b) shear layer with 500× magnification, c) core layer with 100× magnification, and d) core layer with 500× magnification.

layer are irregularly oriented. At RT the fracture surface of the PA6.6 matrix material between the fibers is quite brittle. Fiber extraction and matrix failure are the occurring failure mechanisms. Figure 14(b) visualises good bonding between glass fibers and the matrix material. The found structures are consistent with literature about short fiber reinforced composites.[29,30]

Figure 15 presents the failure surface of a short standardized testing specimen milled from plate transverse to fiber direction ($\theta = 90°$, RT, $R = 0.1$, $N = 285298$). It can be seen in Figure 15(a,b) that fibers in the shear layers are oriented transverse to load direction (in injection moulding direction). Fibers in the core layers [Figure 15(c,d)] do not show distinctive orientation. In the shear layers matrix failure is the dominating failure mechanism because the transversely oriented fibers cannot absorb much load. In the core layer matrix failure as well as fiber extraction occur. The SEM photographs Figure 15(b,d) with 500× magnification additionally illustrate good bonding between glass fibers and PA6.6 matrix.

The influence of high test temperatures on the cyclic material behavior is illustrated by example of a short standardized testing specimen milled from plate transverse to fiber direction ($\theta = 90°$, $T = 150°C$, $R = 0.1$, $N = 1020000$) in Figure 16. The more ductile matrix material behavior at higher temperatures is clearly visible. These observations are consistent with the results of the monotonic tests at high temperatures. With increasing temperature ductility of matrix material increases and matrix material shows a high degree of deformation which results in crazes, voids, and fibrillar structures [Figure 16(b,d)].[30]

Fracture surfaces of injection moulded standardized testing fatigue specimens without weld lines (Figure 17) are compared to specimens with weld lines (Figure 18). In the shear layer of standardized testing specimens without weld lines (RT, $R = 0.1$, $N = 425696$) specimens show fiber orientation in load direction [Figure 17(a,b)]. The core layer is very small compared to short standardized specimens milled from plates and surrounded by the shear layer [Figure 17(c)]. Fiber extraction in the shear layer [Figure 17(a,b)] and brittle matrix failure in the small core area [Figure 17(c,d)] are observed failure mechanisms.

In standardized specimens with weld lines (RT, $R = 0.1$, $N = 328907$), almost all fibers are oriented transverse to the injection moulding direction in the weld line plane [Figure 18(a,b)]. In case of failure, fibers cannot inhibit crack growth.

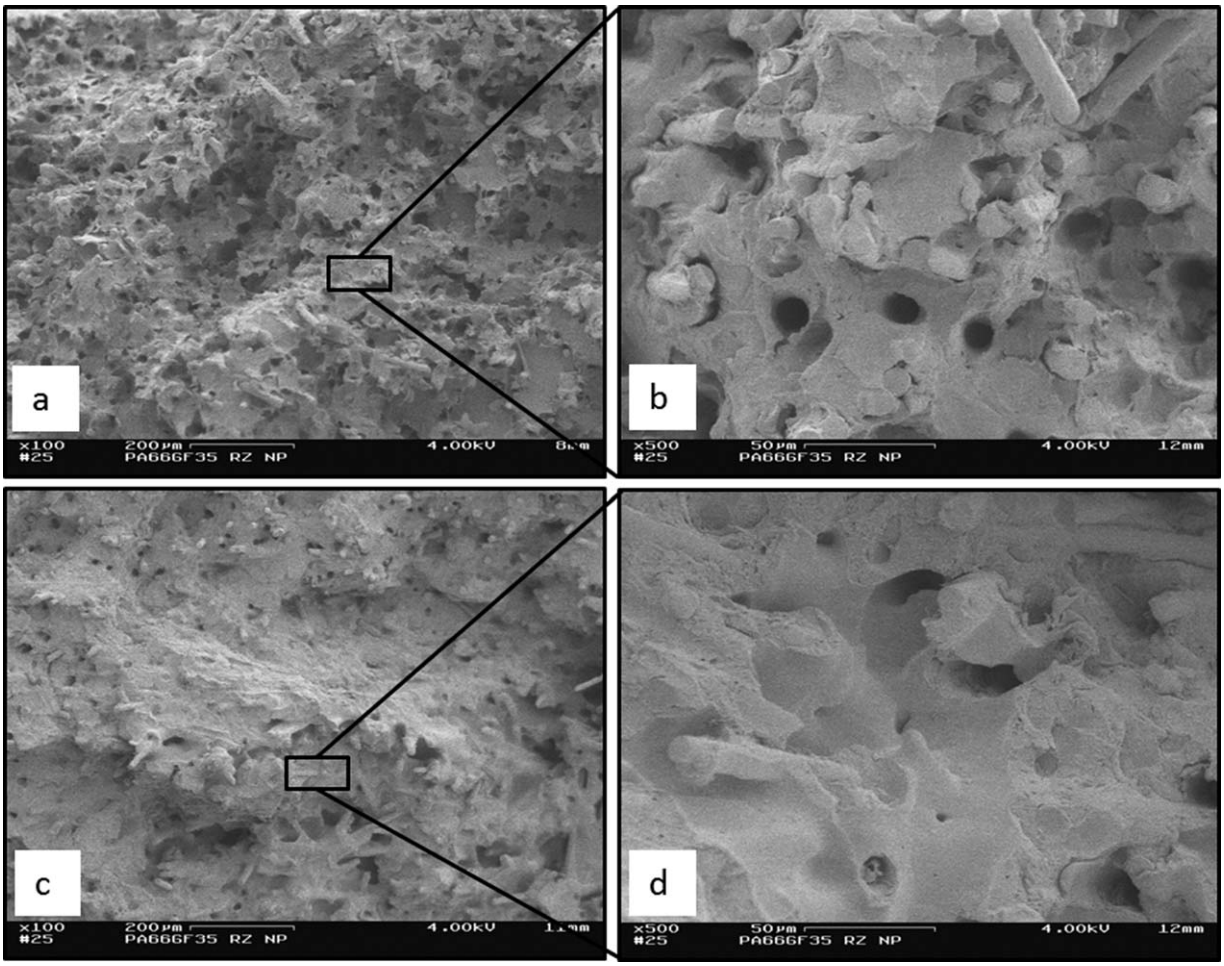

Figure 17. Fracture surface of PA6.6-GF35 standardized fatigue specimen without weld line at RT, $\sigma_a = 45$ N mm^{-2}, $R = 0.1$, $N = 425696$ (shear and core layer): a) shear layer with 100× magnification, b) shear layer with 500× magnification, c) core layer with 100× magnification, and d) core layer with 500× magnification.

Fracture can occur parallel to fiber orientation which results in brittle matrix failure in big parts of the cross section. The fracture surface indicates bad connection between the melt flows that met in the weld line during the injection moulding process. The brittle appearance of the fracture surface is consistent with CT photographs (Figure 13) and with decreased static and

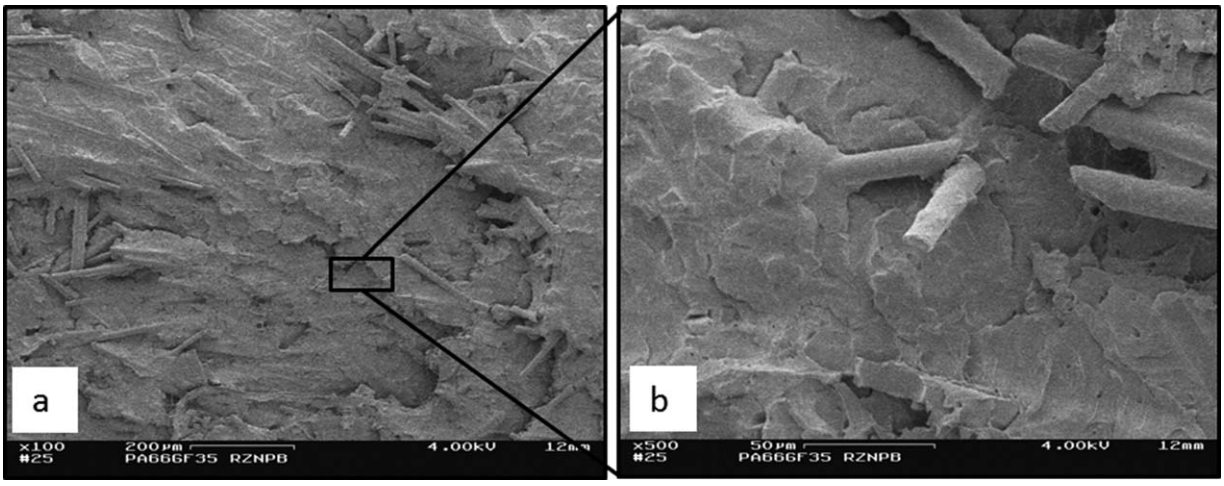

Figure 18. Fracture surface of PA6.6-GF35 standardized fatigue specimen with weld line at RT, $\sigma_a = 20$ N mm^{-2}, $R = 0.1$, $N = 328907$ (shear layer): a) shear layer with 100× magnification and b) shear layer with 500× magnification.

fatigue strengths compared to standardized testing specimens without weld lines.

CONCLUSIONS

In this work, the influences of fiber orientation and weld lines on the morphological structures and damage mechanisms of PA6.6-GF35 under quasistatic and fatigue loads were investigated. Two different specimen types were produced with injection moulding process to create different fiber orientations. The first specimen type was milled from injection moulded plates possessing distinctive shear and core layers across the thickness. As second specimen type standardized testing specimens were injection moulded with and without weld lines. In specimens without weld lines a core layer was surrounded by highly oriented shear layers in the testing cross-section. Tensile and 3-point-bending loads were applied in quasistatic and fatigue tests. Test temperatures were varied between RT and 150°C. Fiber orientations in the intact specimens were characterized with CT. The change of morphological structures depending on fiber orientation and increasing test temperature was studied by investigating fracture surfaces with SEM.

Due to the bigger shear layers in injection moulded standardized specimens compared to short standardized specimens milled from plates (Figure 1), in standardized specimens more fibers were aligned in load direction under tensile loads in the test cross-section. As a consequence, in quasistatic tests Young's moduli and tensile strengths of standardized testing specimens were significantly higher compared to the other specimen geometry. In fatigue tests, nominal stress amplitudes were higher for standardized testing specimens under loading ratios $R = 0.1$ and $R = -1$. High test temperatures decreased mechanical properties in quasistatic tests and halved nominal stress amplitudes in fatigue tests for specimens with fibers aligned in load direction and transverse to load direction. Weld lines decreased the mechanical properties in all tests though the decrease was not as significant under flexural loads as under tensile loads because of the different stress gradients in the specimens.

Specimens with fiber orientation $\theta = 0°$ showed fiber extraction and partially brittle matrix failure as dominating failure mechanisms at RT. For specimens with fiber orientation $\theta = 90°$ and specimens possessing weld lines very brittle fracture surfaces were found. Bonding between polymeric matrix material and glass fiber was found to be good in all investigated specimens. At higher test temperatures, microstructure, and failure mechanisms changed to a more ductile behavior. Microstructures such as crazes and fibrillare structures occured. The influence of changing morphological structures, when testing beyond the glass transition temperature of the polymeric matrix material at test temperatures 90 and 150°C was reflected in the mechanical test results.

The conducted investigations provide input parameters for a fatigue life prediction model based on stress gradient concept developed by Eichlseder.[23] Results of this research emphasize the importance of inclusion of injection moulding process simulation and, thus, knowledge about actual fiber orientation for accurate life time prediction. The implementation of a new fatigue life prediction model considering actual fiber orientation tensors and weld lines for short glass fiber reinforced polyamide 6.6 will be presented in a further article.

ACKNOWLEDGMENTS

The results presented in this article were performed within the funded EU-Cornet project "Advanced PartSim" and had the goal of optimising product development in the early development phases by means of virtual knowledge-based systems. The authors are grateful to the European Union, the Ministry of Education, Science and Technology of the Republic of Slovenia, the Austrian Research Promotion Agency (FFG) as well as the "Otto von Guericke" Confederation of Industrial Research Associations (AIF) and the Federal German Ministry of Economic Affairs and Technology (BMWi) in Germany for the financial support of the "Advanced PartSim" Cornet project. The authors' special thanks also extend to the Upper Austrian University of Applied Sciences for the opportunity of computer tomographic investigations.

REFERENCES

1. Zhou, Y.; Mallick, P. K. *Polym. Compos.* **2006**, *27*, 230.
2. Hull, D.; Clyne, T. W. Cambridge Solid State Science Series, 2nd ed.; Cambridge University Press: Cambridge, New York, **1996**.
3. Horst, J. J. Influence of fibre orientation on fatigue of short glass fibre reinforced polyamide. Ph.D. Dissertation, TU Delft, The Netherlands, **1997**.
4. Sankaran, S.; Mallick, P. K. Influence of injection molding process parameters on fatigue performance of short glass fiber reinforced polyamide-6,6. In ECCM15—15th European Conference on Composite Materials, Venice, Italy, 24–28 June, **2012**.
5. Advani, S. G.; Tucker, Ch. L. *J. Rheol.* **1987**, *31*, 751.
6. Mlekusch, B. *Compos. Sci. Technol.* **1999**, *59*, 547.
7. Davidson, N. C.; Göschel, U.; Eyerer, P. Characterisation of particle filled systems. In Proceedings of 18th Stuttgarter Kunststoff-Kolloquium, **2003**.
8. Hine, P. J.; Duckett, R. A. *Polym. Compos.* **2004**, *25*, 237.
9. Eberhardt, C. N.; Clarke, A. R. *J. Microsc.* **2002**, *64*, 2113.
10. Friedrich, K. *Compos. Sci. Technol.* **1985**, *22*, 43.
11. Hegler, R. P. *Kunststoffe* **1984**, *74*, 271.
12. Erhard, G. Konstruieren mit Kunststoffen. Carl Hanser Verlag: München, **2008**.
13. Zhou, Y.; Mallick, P. K. *Mater. Sci. Eng.* **2005**, *A393*, 303.
14. Selzer, R.; Friedrich, K. *Compos. Part A* **1997**, *28A*, 595.
15. Tokaji, K.; Shiota, H.; Ogawa, T.; Yumitori, S. *J. Mater. Sci.* **1998**, *12*, 4739.
16. Barbouchi, S.; Bellenger, V.; Tcharkhtchi, A.; Castaing, Ph.; Jollivet, T. *J. Mater. Sci.* **2007**, *42*, 2181.
17. Bernasconi, A.; Davoli, P.; Basile, A.; Filippi, A. *Int. J. Fatigue* **2007**, *29*, 199.
18. Sonsino, C.M.; Moosbrugger, E. *Int. J. Fatigue* **2008**, *30*, 1279.
19. Guster, Ch.; Pinter, G.; Eichlseder, W.; Lang, R. W. Effects of temperature and moisture on the tensile/tensile fatigue

behavior of an injection molded sgf-reinforced partial aromatic polyamide. In 12th International Conference on Fracture, Ottawa, Kanada, July 12th–17th, **2009**.

20. De Monte, M.; Moosbrugger, E.; Quaresimin, M. *Compos. Part A* **2010**, *41*, 859.
21. De Monte, M.; Moosbrugger, E.; Quaresimin, M. *Compos. Part A* **2010**, *41*, 1368.
22. Moesenbacher, A.; Guster, Ch.; Pinter, G.; Eichlseder, W. Investigation of concepts describing the influence of stress concentration on the fatigue behaviour of short glass fibre reinforced polyamide. In ECCM15—15th European Conference on Composite Materials, Venice, Italy, 24–28 June, **2012**.
23. Eichlseder, W. *Comput. Struct.* **2002**, *80*, 2109.
24. Guster, Ch.; Pinter, G.; Mösenbacher, A.; Eichlseder, W. *Proc. Eng.* **2011**, *10*, 2104.
25. DIN EN ISO 527-2. European Committee for Standardization: Brussels, Belgium, **1996**.
26. DIN EN ISO 527-1. European Committee for Standardization: Brussels, Belgium, **1996**.
27. DIN EN ISO 178. European Committee for Standardization: Brussels, Belgium, **2006**.
28. ASTM E739-91. ASTM International: West Conshohocken, PA, **1991**.
29. Lang, R.W. Applicability of linear elastic fracture mechanics to fatigue in polymers and short-fiber composites. Ph.D. Dissertation, Lehigh University: Bethlehem, Pennsylvania, **1984**.
30. Novotny, M.M. Fatigue crack propagation in engineering thermoplastics – Effects of temperature and short fiber reinforcement. Ph.D. Dissertation, University of Leoben: Leoben, Austria **1997**.